NANO LETTERS

2004
Vol. 4, No. 12
2389−2392

Nanoparticle Networks on Silicon: Self-Organized or Disorganized?

Christopher P. Martin,* Matthew O. Blunt, and Philip Moriarty

School of Physics & Astronomy, The University of Nottingham, University Park, Nottingham, NG7 2RD, United Kingdom

Received September 7, 2004; Revised Manuscript Received October 12, 2004

ABSTRACT

A structural motif that appears very frequently not only in a wide range of nanostructured systems but also on mesoscopic to macroscopic length scales is the "cellular network". We present a quantitative analysis of the morphology of cellular networks formed by thiol-passivated Au nanoparticles, and, for comparison, organometallic molecules, spin cast onto native oxide-terminated silicon substrates. The structural parameters determined from Voronoi tessellation and Minkowski functional analyses of the experimental data are compared to those extracted from Monte Carlo simulations of nanoparticle network formation. The key result of this comparative study is that although the cell positions are spatially correlated, i.e., they deviate strongly from those expected for a Poisson point set, this correlation arises simply from a coalescence of neighboring cells during network formation. Complex nonlinear processes such as spinodal decomposition or Marangoni convection are therefore not *always* a prerequisite for the formation of spatially correlated networks.

The patterning of surfaces using nonlithographic techniques, such as those that exploit the dewetting of thin films, has immense potential for large-scale fabrication of the next generation of inexpensive electronic devices. When the specific balance of interfacial energies causes a film on a substrate to break up, the rupture frequently occurs on a well-defined length scale. The result is generally a large area that contains features of uniform size. This is also true of initially homogeneous mixtures that separate into two phases. In addition to their possible electronic applications, the physical and chemical properties of these nanostructured materials may prove to have important applications in areas such as catalysis and materials science. Wetting, dewetting, and phase-separating polymer systems have been studied extensively, and a comprehensive review is presented by Geoghegan and Krausch.[1]

It is important to note that the emergence of a well-defined correlation length is not limited to dewetting films and phase separation. A wide range of apparently different systems appear to exhibit a preferred length scale for pattern formation. Patterns on the hides of animals, cellular structures formed by drying and cracking mud, and the arrangement of domains in a magnetic material are all examples. In this letter, however, we shall focus on patterns similar to those observed in dewetting films. In particular, structures resembling dewetted polymers have been observed in the drying-mediated self-assembly of CdSe nanoparticles,[2] and within our own group, Au nanoparticles.[3] These structures have also been convincingly reproduced by MC simulation using basic thermodynamic principles, as shall be discussed later.[4] It is perhaps not surprising that the patterns observed in nanoparticle self-assembly are similar to those observed in dewetting polymer systems. The evaporation of a solvent is likely to be influenced by the same factors as a dewetting liquid; local film thickness fluctuations and small temperature differences are almost certain to play a part in both systems. This does not, however, go any way toward explaining why, as we shall show below, patterns with quantitatively very similar degrees of order are formed in each system.

The appearance of a ring in the two-dimensional Fourier transform is frequently cited as evidence for long-range ordering.[5−11] There is still considerable debate on this topic, particularly relating to polymer films,[10−12] where the dewetting patterns tend to be attributed to one of two processes: nucleation and growth of holes, or some type of spinodal process. It seems likely that different systems, and in fact the same system under different conditions (as suggested by Bischof et al.[13] and Xie et al.[9]), can probably evolve by either mechanism. It would therefore be convenient if we could examine a pattern and determine from its morphology alone its probable origin.

There are a number of analytical tools that can be applied to a pattern to characterize it numerically. These techniques are especially useful where the structure is cellular, or conversely, where it consists of a number of separate droplets (as used by Brinkmann et al.[14]). Comparing such distributions of objects with a random (Poisson) distribution can give us an insight into the degree of order (or disorder) of the system. The Voronoi tessellation has been used to indicate deviations

10.1021/nl048536w CCC: $27.50
Published on Web 10/30/2004

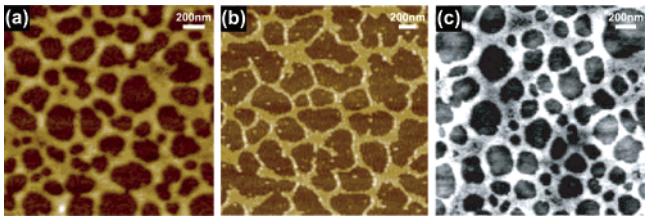

Figure 1. Three AFM images from experiments, showing (a) area of dewetted organometallic clusters, (b) Au nanoparticle networks on silicon, and (c) a polystyrene (PS) layer spin-coated from solution in toluene (from [11]). Panel (c), by P. Müller-Buschbaum, used with permission. © 2003 IOP Publishing Ltd.

from Poisson statistics in cellular nanoparticle networks.[3] More recently, we have used "Minkowski morphometry" (as described by Michielsen and de Raedt[15]) to indicate that the dewetting centers of organometallic clusters on silicon appear to be nonrandom.[16] Performing simulations and comparing the final results using both statistical crystallography and Minkowski morphometry can lead us to a better understanding of what clues we can use to identify the formation mechanisms of real systems.

Figure 1 shows three images from different experimental systems. Panel (a) shows a dewetting pattern in organometallic clusters on silicon. Statistical analysis of this structure initially suggests that it could result from an ordered formation mechanism.[16] Both the Voronoi tessellation and Minkowski functional grain growth analysis show a strong deviation of the distribution of cell centers from a random distribution. The entropy of the tessellation (defined as $S = -\sum_n P_n \ln P_n$, where P_n is the probability of a cell having n sides) is 1.38, compared to the expected value of 1.71 for a Poisson distribution. Furthermore, the second moment about the mean (or variance, μ_2) of the number of cell sides is lower than expected, at 1.03. A Poisson distribution is associated with a variance of 1.78.

Many Au nanoparticle networks similar to those in panel (b) have been examined in our group, and again, numerically similar deviations from Poisson statistics have been highlighted using the Voronoi tessellation.[3] Panel (c) shows a section of a polystyrene (PS) dewetting pattern,[11] which is extremely similar to the structure in panel (a). The same deviations from disorder are seen time and again across many systems, and these are just a few examples. So are these structures the result of some kind of universal ordering, or could there be another explanation? The study of nanoparticle simulations can provide new perspective on the topic.

The model used for our simulations is based on that of Rabani et al.,[4] whereby the solvent is represented as a two-dimensional lattice gas, and fluctuations in solvent density are controlled by the Metropolis algorithm.[17] In brief, each cell of a square lattice, i, may contain either liquid ($l_i = 1$), vapor ($l_i = 0$), or nanoparticle ($n_i = 1$), and the presence of a nanoparticle excludes the presence of solvent. A single lattice site represents a square of side 1 nm (approximately equal to the correlation length, ξ, of the solvent), and the particles are represented by squares of side 3 nm.

To perform the simulation, each solvent cell is examined in turn, and an attempt is made to convert the cell from liquid to vapor (or vice-versa) with an acceptance probability $p_{acc} = \min[1, \exp(-\Delta H/k_B T)]$, where ΔH is the change in energy that would result from such a conversion. This energy change is calculated from the total energy of the system:

$$H = -\epsilon_l \sum_{<ij>} l_i l_j - \epsilon_n \sum_{<ij>} n_i n_j - \epsilon_{nl} \sum_{<ij>} n_i l_j - \mu \sum_{il_i} \qquad (1)$$

where ϵ_l, ϵ_n, and ϵ_{nl} are the attraction strengths between two adjacent sites that are occupied by solvent, nanoparticle, or solvent and nanoparticle, respectively. The equilibrium state of the solvent is defined by μ, the chemical potential, and T, the temperature of the system. As observed in our experiments, the final morphology of a pattern is controlled mainly by the vapor pressure of the solvent, the particle concentration, and the particle mobility (resulting from particle−substrate interactions). Other factors such as humidity were not controlled during experiments and have not been included in the simulations. Although our recent experiments suggest that humidity may play a (secondary) role in nanoparticle organization, the AFM data described here are reproducible for a wide range of samples prepared under conditions of different ambient humidity. (Note that recent light scattering experiments[18] carried out during spin coating of the solvent−nanoparticle film indicate that the drying process takes of order 1 s.)

Our simulations differ from those of Rabani et al., in that not only nearest but also next-nearest neighbors are taken into account when calculating the energy change associated with a particular solvent transition. This modification was necessary to compensate for anisotropy observed in the heterogeneous limit of slow, nucleation-driven evaporation. Without the inclusion of next-nearest neighbor interactions, vapor "bubbles" tend to form as squares with their sides aligned to the lattice. This is simply because a solvent cell on a liquid-vapor interface that is diagonal (at 45° to the square lattice) has two liquid nearest neighbors, rather than three in the case of a horizontal or vertical interface. Hence diagonal interfaces are less stable and tend to retreat rapidly until they form the corner of a square. This is clearly an unnatural state of affairs, as in reality the solvent is an isotropic medium, which should result in vapor bubbles that are approximately circular.

To implement this modification, the first and third terms of eq 1 are calculated over eight neighbors, with the next-nearest neighbors being given a weighting of $1/\sqrt{2}$, as opposed to unit weighting for the nearest neighbors. A renormalization factor is also introduced for these terms, so that the same parameters can be used as in the nearest neighbor model and the results compared directly. This was manually determined to be 0.562 by matching the nucleation rate in the heterogeneous regime.

As in the Rabani model, the nanoparticles perform a random walk on the lattice, and are only able to move into "wet" areas of the substrate. The effective particle mobility is controlled by the number of times each particle is examined in one solvent cycle. This ratio of particle steps to solvent steps, the "mobility ratio" (MR), takes values between 10 and 70 in our simulations.

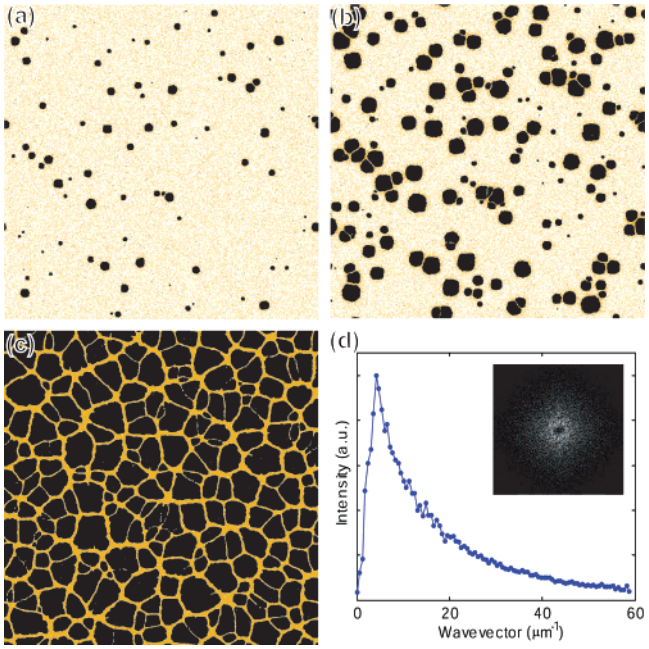

Figure 2. Results from the heterogeneous (nucleation) regime, with $k_BT = \epsilon_l/4$, $\epsilon_n = 2\epsilon_l$, $\epsilon_{nl} = 1.5\epsilon_l$, $\mu = -2.25\epsilon_l$, MR = 30, and a nanoparticle coverage of 20%, showing the early stages of pattern formation in a 4008 × 4008 pixel system after (a) 99 MC steps, with a distribution of nucleation sites that is clearly uncorrelated, (b) 199 MC steps, illustrating coalescence of neighboring nucleation sites, and (c) 899 MC steps, the stable end result, which is best described as a cellular network. Pane (d) shows a radially averaged two-dimensional Fourier transform of (c), with a clear peak resulting from the ring visible in the inset.

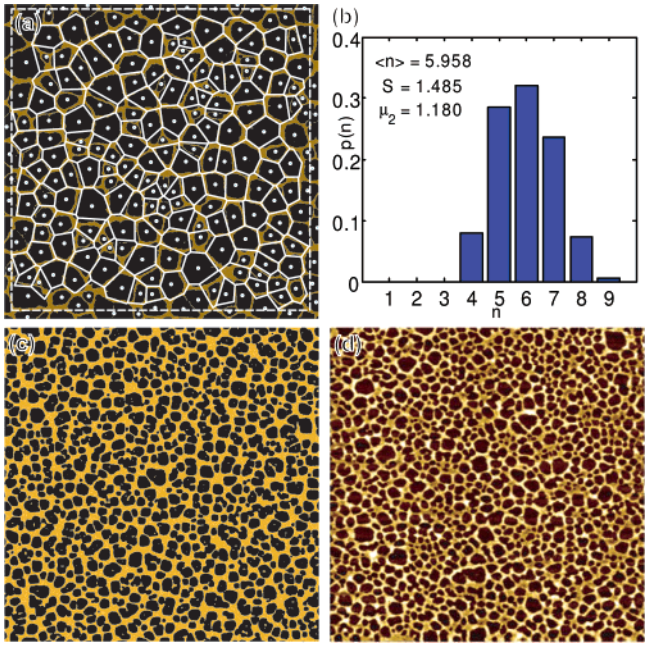

Figure 3. Statistical analysis showing (a) a Voronoi tessellation of Figure 2(c) highlighting the cellular structure and (b) a graph indicating the probability of a cell having a given number of sides in the tessellation. Panel (c) shows another simulation image, this time 3000 × 3000, $k_BT = \epsilon_l/3$, MR = 50, and a coverage of 35%, and panel (d) is an 8 μm area of dewetted organostannoxane clusters (from which 1(a) was taken), shown alongside panel (c) for ease of comparison. The qualitative similarity between these two images is striking.

Figure 2 shows three frames from one of our simulations, along with a radially averaged two-dimensional Fourier transform of the final frame. It is apparent from panel (a) that the nucleation sites are uncorrelated; the vapor bubbles are clustered in some areas, and other areas have little or no nucleation. This is not surprising, as the program dynamics are entirely stochastic and do not take into account any interactions beyond the next-nearest neighbors. In panel (b), we can see the bubbles have expanded somewhat, and several have collided with other bubbles, either leaving a thin wall of particles, or in some cases almost completely merging together to leave only isolated particle groups. In the final frame (c), the structure is foam-like and best described as a cellular network. Qualitatively, this structure appears ordered, much like many that have been observed in experiments, and it is similar to Figure 1(b). More importantly, the two-dimensional Fourier transform (d) reveals the familiar ring which is often cited as evidence for long-range ordering. This is clearer from the radial average, which has a very distinct peak.

As a more quantitative examination of the same pattern, Figure 3(a) shows a Voronoi tessellation of the final structure, along with Figure 3(b) a plot of the probability of finding a cell with a given number of sides. This interestingly reveals an entropy of 1.48, which is not quite as low as the organostannoxane network but still significantly lower than the Poisson value. In this instance, it is also worth noting that the number of cells is considerably smaller than in the sample used for the organostannoxane calculations, so the error in this measure is larger.

Panels (c) and (d) of Figure 3 show another simulation image, alongside the AFM image of the dewetting pattern of organometallic clusters on silicon from Figure 1(a). When compared, the two images appear to have very much in common. Moreover, when Minkowski functional grain growth analysis is applied to the simulation image, the resulting plots are virtually indistinguishable from those obtained from the experimental image. Figure 4(a−c) shows these plots of the area (A), perimeter (U), and Euler characteristic (χ) as a function of the normalized edge length of square grains for both images. It is clear that the plots follow each other very closely, as do the difference plots, (d−f).

Tessellation analysis of the simulation image gives values of variance and entropy that correspond to those of the organostannoxane networks to within one decimal place ($\mu_2 = 1.03$ and $S = 1.41$). Although the systems are different, in that our simulation patterns result from evaporation and the patterns in (d) result from dewetting, their morphology is not only qualitatively similar but also *quantitatively indistinguishable* within reasonable error margins.

Our simulations are completely stochastic. The patterns produced are known to be the result of random nucleation due to local thermal fluctuations, yet there still appears to be some kind of ordering. Put together, this evidence points strongly to one conclusion: deviation from Poisson statistics, and the appearance of a well-defined correlation length, does

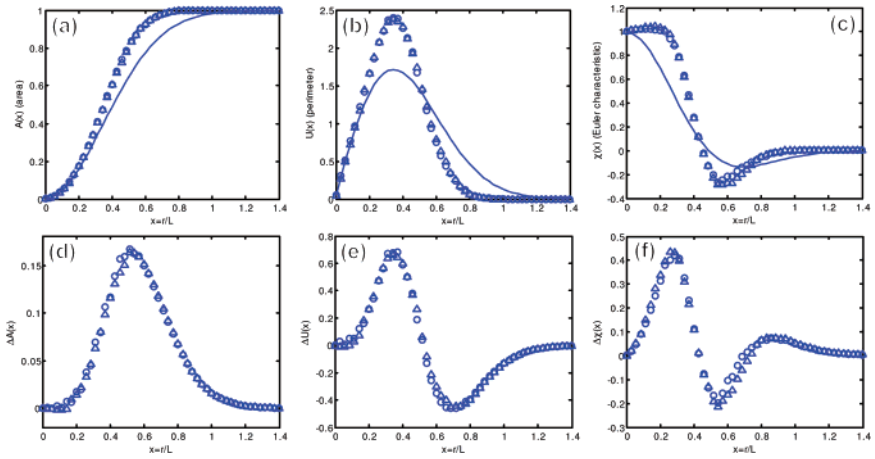

Figure 4. Minkowski functional grain growth analysis for the organostannoxane dewetting pattern (open circles) and the simulated nanoparticle image of Figure 3(c) (triangles). Panels (a−c) show the plots of area, perimeter, and Euler characteristic respectively, with the expected behavior for a Poisson distribution shown by the solid line. Panels (d−f) show the deviation from the Poisson lines in each case. It is clear that not only do both patterns have a strong deviation from the Poisson distribution but they also follow each other quite closely.

not necessarily indicate an ordered formation mechanism. So how do these deviations arise when the processes involved are known to be entirely stochastic? Brinkmann et al. raised the question of the origin of apparent ordering in Alq_3 droplet on H-terminated Si(100),[14] and came to conclusions based on droplet coalescence. Although the droplet system is almost the inverse of those systems presented here, similar reasoning may apply. Observing the progress of our simulations has led us to propose the following suggestion for a possible mechanism.

First, in a nucleation-driven dewetting or evaporation scenario, it is understood that the system conditions (temperature, volatility, or the balance of interfacial energies and viscosity) will lead to a specific nucleation rate. That is to say, there will be a certain number of nucleation events per unit area per unit time. As vapor bubbles (or dewetting centers) expand, there will be a smaller area available for nucleation. Furthermore, the area remaining will be less likely to host a nucleation event as the concentration of particles (or the thickness of the film) will be proportionally greater. As a result, the nucleation rate will drop off relatively rapidly as the holes in the film expand. This means there is a limited time window in which nucleation can occur. This reduces the maximum possible size of a vapor bubble and also narrows the overall hole size distribution.

Second, nucleation occurring close to the edge of an existing vapor bubble, or the coincidence of several nucleation events in the same region, will generally lead to a coalescence event. The degree to which this coalescence occurs will depend on the dynamics of the system; in a system containing particles that are highly mobile (or a fluid that has a low viscosity and a strong dislike for the substrate) coalescence of holes is much more likely. An important point to note however, is that the closer together two nucleation events are (in both space and time), the more likely the resulting holes are to coalesce. This will effectively "wipe out" the clustering that is inherent in a Poisson distribution, even in a relatively immobile or viscous system.

These two points lead directly to the result that is seen so often: a cellular structure, with a narrow distribution of cell sizes, and a low degree of small-cell clustering. We cannot say definitively that structures that display these characteristics are not the result of spinodal processes, but it seems clear that deviations from Poisson statistics do not provide sufficient evidence for long-range ordering.

Supporting Information Available: Figure 1 regarding the inclusion of next-nearest neighbors in simulations. This material is available free of charge via the Internet at http://pubs.acs.org.

References

(1) Geoghegan, M.; Krausch, G. *Prog. Polym. Sci.* **2003**, *28*, 261−302.
(2) Ge, G.; Brus, L. *J. Phys. Chem. B* **2000**, *104*, 9573−9575.
(3) Moriarty, P.; Taylor, M. D. R.; Brust, M. *Phys. Rev. Lett.* **2002**, *89*, 248303.
(4) Rabani, E.; Reichman, D. R.; Geissler, P. L.; Brus, L. E. *Nature* **2003**, *426*, 271−274.
(5) O'Shea, J. N.; Phillips, M. A.; Taylor, M. D. R.; Moriarty, P. *Appl. Phys. Lett.* **2002**, *81*, 5039−5041.
(6) Reiter, G. *Langmuir* **1993**, *9*, 1344−1351.
(7) Schlagowski, S.; Jacobs, K.; Herminghaus, S. *Europhys. Lett.* **2002**, *57*, 519−525.
(8) Müller-Buschbaum, P.; Gutmann, J. S.; Lorenz-Haas, C.; Wunnicke, O.; Stamm, M.; Petry, W. *Macromolecules* **2002**, *35*, 2017−2023.
(9) Xie, R.; Karim, A.; Douglas, J. F.; Han, C. C.; Weiss, R. A. *Phys. Rev. Lett.* **1998**, *81*, 1251−1254.
(10) Higgins, A. M.; Jones, R. A. L. *Nature* **2000**, *404*, 476−478.
(11) Müller-Buschbaum, P. *J. Phys.: Condens. Matter* **2003**, *15*, R1549−R1582.
(12) Jacobs, K.; Herminghaus, S.; Mecke, K. R. *Langmuir* **1998**, *14*, 965−969.
(13) Bischof, J.; Scherer, D.; Herminghaus, S.; Leiderer, P. *Phys. Rev. Lett.* **1996**, *77*, 1536−1539.
(14) Brinkmann, M.; Graff, S.; Biscarini, F. *Phys. Rev. B* **2002**, *66*, 165430.
(15) Michielsen, K.; De Raedt, H. *Phys. Rep.* **2001**, *347*, 461−538.
(16) Frehill, F.; Schulte, K. H. G.; Martin, C. P.; Wang, L.; Patel, S.; Purton, J. A.; Vos, J. G.; Moriarty, P. *Langmuir* **2004**, *20*, 6421−6429.
(17) Metropolis, N.; Rosenbluth, A. W.; Rosenbluth, M. N.; Teller, A. H.; Teller, E. *J. Chem. Phys.* **1953**, *21*, 1087−1092.
(18) Blunt, M. O.; Martin, C. P.; Heriot, S. K.; Geoghegan, M.; Moriarty, P., unpublished, 2004.

NL048536W